

# ECOLOGICAL DESIGN OPTIMIZATION OF NOZZLE PARAMETERS FOR BURNISHING OPERATION

Minh-Thai Le<sup>1</sup>, An-Le Van<sup>2,\*</sup>, Trung Thanh Nguyen<sup>3</sup>, Xuan-Ba Dang<sup>4</sup>

<sup>1</sup> Faculty of Special Equipments, Le Quy Don Technical University, Hanoi, Vietnam

<sup>2</sup> Faculty of Engineering and Technology, Nguyen Tat Thanh University, Ho Chi Minh City, Vietnam

<sup>3</sup> Faculty of Mechanical Engineering, Le Quy Don Technical University, Hanoi, Vietnam

<sup>4</sup> Department of Automatic Control, Ho Chi Minh City University of Technology and Education, Ho Chi Minh City, Vietnam

\* ivan@ntt.edu.vn

The design configuration of the nozzle has a vital role in the performance measures of the machining processes. However, parameter optimizations are primary considerations of published works. This study optimizes nozzle design parameters to minimize environmental impacts and enhance the surface quality for the diamond burnishing (DB) operation. The performance measures considered are energy efficiency (ED), noise emission (NE), and the total height of profile roughness (Rt). The variables are the inner diameter (D), spraying distance (S), and pitch angle (P). The optimal Taguchi-based Bayesian regularized feed-forward neural network (TBRFFNN) was applied to propose performance models. The CRITIC approach is utilized to compute the weight values of responses, while the desirability approach (DA) is employed to select optimality. The observed results of the D, S, and P were 3.0 mm, 15 mm, and 45 deg., respectively. The ED was enhanced by 12.7%, while the Rt and NE were decreased by 24.4% and 9.1%, respectively, as compared to the original design parameters. The obtained outcomes could be utilized in the practice to boost technical characteristics. The developed optimizing approach could be employed to deal with optimization problems for different machining processes.

Keywords: nozzle parameters, design optimization, diamond burnishing, ANN, desirability approach

## 1 INTRODUCTION

The DB operation is a prominent finishing approach to improve the properties of different surfaces, in which the burnishing force of the diamond tool is applied to produce the material compression. Low roughness, high hardness, high compressive residual stress, and improved resistance are primary advantages. Other advantages are the simple device, less auxiliary equipment, and longer life of the burnishing tool. Consequently, the DB operation can be utilized in for machining ferrous and non-ferrous materials in the soft stage.

Improving technological indicators of different DB operations has been addressed by many investigators. Optimal burnishing parameters under the cryogenic condition, such as speed ( $V_b$ ), feed ( $f_r$ ), and force ( $f_b$ ) were selected to decrease the average roughness ( $R_a$ ) and surface hardness ( $H_s$ ) [1]. The results indicated that the optimal values of the  $V_b$ ,  $f_r$ , and  $f_b$  were 72.8 m/min, 0.047 mm/rev., and 149.6 N, respectively. The optimal  $R_a$  (0.2  $\mu$ m) and  $H_s$  (398 HV) of the burnished 17-4 hardened stainless could be obtained using the response surface method (RSM) [2]. A sustainable diamond burnishing under the minimum quantity lubrication (MQL) condition was developed to enhance the  $R_a$  and  $H_s$ , in which the optimizing values of the  $R_a$  and  $H_s$  were 0.068  $\mu$ m and 362.8 HV, respectively [3]. The optimal surface roughness (0.11  $\mu$ m) and the fatigue value (506 MPa) for the burnished Cr4 steel could be achieved using a hybrid diamond burnishing [4]. Maximov et al. indicated that the tip radius and the  $f_b$  had the strongest effects on the residual stresses for the burnished 41Cr4 steel [5]. Duncheva et al. emphasized that the diamond burnished surface was significantly improved in terms of wear resistance, as compared to the fine turning, while the geometrical characteristics had significant impacts on the lubrication of the burnished surface [6]. Duncheva et al. stated that the surface characteristics (hardness and texture) were effectively enhanced with the support of internal diamond burnishing [7]. A simulation model using the DEFORM software was developed to capture the roughness value of the DB process [8]. The acceptable errors between the simulated and experimental results indicated the proposed model was reliable. Duncheva et al. emphasized that the DB operation effectively helped to increase the residual stress and micro-hardness on the surface layer of the burnished CuAl8Fe3 aluminum bronze [9]. Moreover, the mirror surfaces and grain-refined microstructures were produced. The wear resistance of the burnished CuAl9Fe4 bronze could be enhanced by 2.6 times, compared to the fine turning process [10]. Furthermore, the DB process significantly decreased the 3D height of the surface roughness. Maximov et al. indicated that an increase in the percentage of the martensitic phase leads to higher fatigue strength of the burnished AISI 304 steel [11]. Moreover, the initial characteristics, including the roughness, micro-hardness, and residual stresses had significant impacts on the surface integrity.

Recently, environmental indicators have been considered by many researchers for different burnishing operations. The energy efficiency of the internal burnishing was enhanced by 7.0%, while the noise emission and  $R_s$  were decreased by 2.2%, and 25.0% [12]. Nguyen and Le revealed that the energy consumption and  $R_s$  of the external burnishing were reduced by 33.0% and 16.0%, respectively [13]. Nguyen et al. stated that the total energy, mean roughness, and roundness of the MQL-assisted internal burnishing were reduced by 12.0%, 14.0%, and 43.0%,

respectively [14]. The carbon emissions, air pollution, and maximum roughness of the DB process of the carbon steel were decreased by 3.8%, 26.5%, and 34.3% using the optimal factors [15]. Moreover, the total burnishing cost was decreased by 11.6% at the selected solution. However, the shortcomings of works related to the diamond burnishing process can be listed as follows:

Practically, the design parameters of the nozzle have serious impacts on the burnishing responses. Therefore, it is necessary to consider the nozzle factors are important inputs. The impacts of nozzle parameters, including the inner diameter, pitch angle, and spray distance on the environmental indicators have not been explored.

The energy efficiency and noise emission of the diamond burnishing operation have been not addressed and optimized. The selection of nozzle parameters to minimize the environmental impacts and boost the machining quality for the diamond burnishing operation has not been executed.

## 2 OPTIMIZATION APPROACH

Three design parameters of the nozzle, including the inner diameter ( $D$ ), spraying distance ( $S$ ), and pitch angle ( $P$ ) are presented in Table 1. The values of the  $D$ ,  $S$ , and  $P$  are selected using the recommendations of the manufacturer of the MQL system and verified with the aforementioned publications. Fig. 1 presents the illustration of nozzle parameters.

Three performance measures, including the energy efficiency of the diamond burnishing process ( $ED$ ), the total height of the roughness profile ( $Rt$ ), and noise emission ( $NE$ ) are considered and optimized. Therefore, an optimization problem is expressed as:

Maximize the  $EF$ ; Minimize the  $Rt$  and  $NE$ .

Constraints:  $1 \leq D \leq 3$  mm;  $15 \leq S \leq 45$  mm;  $30 \leq P \leq 60$  deg.

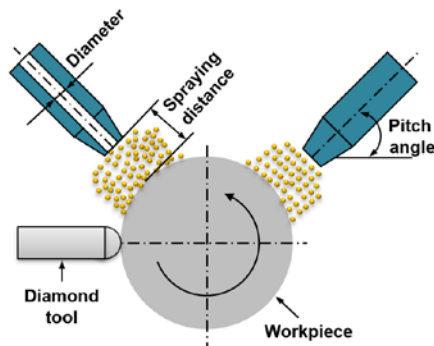


Fig. 1. The scheme of the nozzle parameters

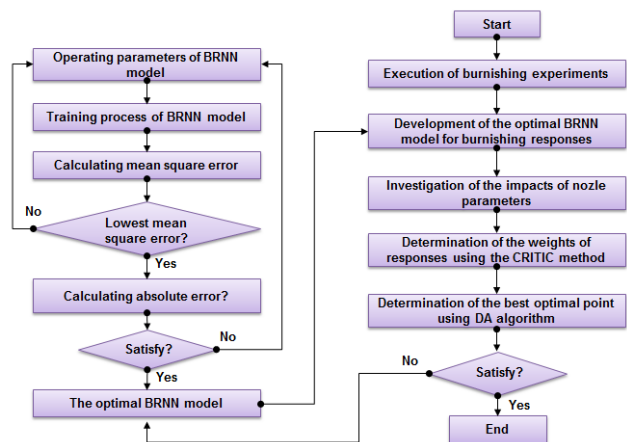


Fig. 2. Optimization approach

The optimizing approach for a new DB operation is depicted in Fig. 2, which is expressed as:

Step 1: The burnishing trials are executed using the full design of the experiment [16, 17].

The  $ED$  value is computed as:

$$ED = \frac{BP}{NP} \tag{1}$$

where  $BP$  and  $MP$  present the machining power in the burnishing time and total power consumed of the machine tool, respectively.

The  $Rt$  value is calculated as:

$$Rt = \frac{\sum_{i=1}^n Rt_i}{n} \tag{2}$$

where  $Rt_i$  is the height of the roughness at the  $i$ th position.

The  $NE$  value is calculated as:

$$NE = \frac{\sum_{i=1}^n NE_i}{n} \tag{3}$$

where  $NE_i$  is the noise emission at the  $i$ th time measured.

Step 2: The correlations of the  $ED$ ,  $NM$ , and  $Rt$  are proposed using the BRFFNN [18, 19].

The BRFFNN requires the Hessian matrix of the objective functions, in which the quadratic function  $\hat{f}$  produced using the Levenberg-Marquardt algorithm. The objective function is expressed as:

$$F = \alpha E_W + \beta E_D \quad (4)$$

where  $E_W$  and  $E_D$  are the sum of squares for weights and the sum of squared errors, respectively.  $\alpha$  and  $\beta$  are objective function parameters.

For the BRFFNN, the weights of the network are considered random variables. The density function of network weights is expressed as:

$$f(w|d, \alpha, \beta, M) = \frac{f(D|w, \beta, M)f(w|\alpha, M)}{f(D|\alpha, \beta, M)} \quad (5)$$

where  $D$  and  $M$  present the obtained data and the particular neural network, respectively.  $f(w|\alpha, M)$  is the prior density. When the Gaussian function is employed, the likelihood -  $f(D|w, \beta, M)$  is expressed as:

$$f(D|w, \beta, M) = \frac{1}{\left(\frac{\pi}{\beta}\right)^{n/2}} e^{-\beta E_D} \quad (6)$$

The normalized likelihood  $f(D|\alpha, \beta, M)$  is expressed as:

$$P(D|\alpha, \beta, M) = \frac{1}{\left(\frac{\pi}{\alpha}\right)^{N/2}} e^{-\alpha E_W} \quad (7)$$

The density model is expressed as:

$$f(w|D, \alpha, \beta, M) = \frac{1}{Z_F(\alpha, \beta)} e^{-(\alpha E_W + \beta E_D)} \quad (8)$$

To observe the optimal architecture of the BRFFNN model, the mean square error ( $MSE$ ) is applied, which is expressed as:

$$MSE = \frac{1}{N} \sum_{i=1}^N (AD - PD)^2 \quad (9)$$

where  $AD$  and  $PD$  present experimental and predictive values, respectively.  $N$  denotes the number of testing points. The best TBRFFNN architecture is chosen with the lowest  $MSE$  value.

Step 3: The CRITIC method is utilized to select computed weights.

The normalized value of each objective ( $x_{ij}$ ) is calculated as:

$$x_{ij} = \frac{x_{ij} - x_j^{word}}{x_j^{best} - x_j^{word}} \quad (10)$$

The standard deviation ( $s_j$ ) of each response is calculated as:

$$s_j = \sqrt{\frac{(\sum_{i=1}^m x_{ij} - x_m)^2}{m-1}} \quad (11)$$

Computation of measure of the conflict ( $I_j$ ):

$$I_j = \sum_{k=1}^m (1 - r_{jk}) \quad (12)$$

Determination of the quantity of the information ( $C_j$ ):

$$C_j = s_j \sum_{k=1}^m (1 - r_{jk}) \quad (13)$$

The computed weight ( $\omega_i$ ) of the burnishing response is calculated as:

$$\omega_i = \frac{C_j}{\sum_{k=1}^n C_j} \quad (14)$$

Step 4: The DA is utilized to find optimal outcomes.

With a higher aim, the desirability value ( $d_i$ ) is computed as:

$$d_i = \begin{cases} 0, Y_i \leq LR_i \\ \left(\frac{Y_i - LR_i}{HR_i - LR_i}\right)^\omega, LR_i < Y_i < HR_i \\ 1, Y_i \geq HR_i \end{cases} \quad (15)$$

With a lower aim, the  $d_i$  is computed as:

$$d_i = \begin{cases} 0, Y_i \leq LR_i \\ \left(\frac{HR_i - Y_i}{HR_i - LR_i}\right)^\omega, LR_i < Y_i < HR_i \\ 1, Y_i \geq HR_i \end{cases} \quad (16)$$

With the aimed purpose, the  $d_i$  is computed as:

$$d_i = \begin{cases} \left(\frac{Y_i - LR_i}{TP_i - LR_i}\right)^{\omega_1}, LR_i < Y_i < TP_i \\ \left(\frac{Y_i - HR_i}{TP_i - HR_i}\right)^{\omega_2}, TP_i < Y_i < HR_i \\ 0, otherwise \end{cases} \quad (17)$$

With the range aim, the  $d_i$  is computed as:

$$d_i = \begin{cases} 1, LR_i < Y_i < HR_i \\ 0, otherwise \end{cases} \quad (18)$$

where  $LR_i$ ,  $HR_i$ , and  $TP_i$  present the low, high, and targeted responses, respectively.  $\omega_i$  presents the assigned weight.

The total desirability value ( $D$ ) is computed as:

$$DA = \left( \prod_{i=1}^m d_i^{\omega_i} \right)^{1/\sum \omega_i} \quad (19)$$

### 3 EXPERIMENTAL SETTING

The diamond burnishing experiments are performed using a conventional turning machine (Fig. 3). The diamond burnishing tool is firmly held on the tool post. The round bar entitled AISI 4140 steel is fixed between live and dead centers. Each specimen has a diameter of 80.0 mm and a length of 130.0 mm. Table 2 presents the chemical compositions of the AISI 4140. The lubricant is pumped using the electrical pump, while the frequency generator is applied to control the flow rate. The compressed air is transferred from the MQL system to the double vortex tubes for decreasing the working temperature.

A power sensor labeled CA 8333 produced by Chauvin Arnoux is utilized to measure the power consumed, while a Mitutoyo SJ-301 is applied to capture the roughness value. A smart sound meter entitled ST9604 is employed to obtain the noise emission during machining time.

The exemplary data of the power consumed, average roughness, and noise is shown in Fig. 4.

Table 1. Design parameters

Parameters	Ranges
Inner diameter-D (mm)	1-2-3
Spraying distance-S (mm)	15-30-45
Pitch angle-P (deg.)	30-45-60

Table 2. Chemical compositions of AISI 4140 steel

Element	Cr	Mn	C	Si	Mo	S	P	Fe
%	1.00	0.90	0.41	0.25	0.18	0.04	0.035	Balance

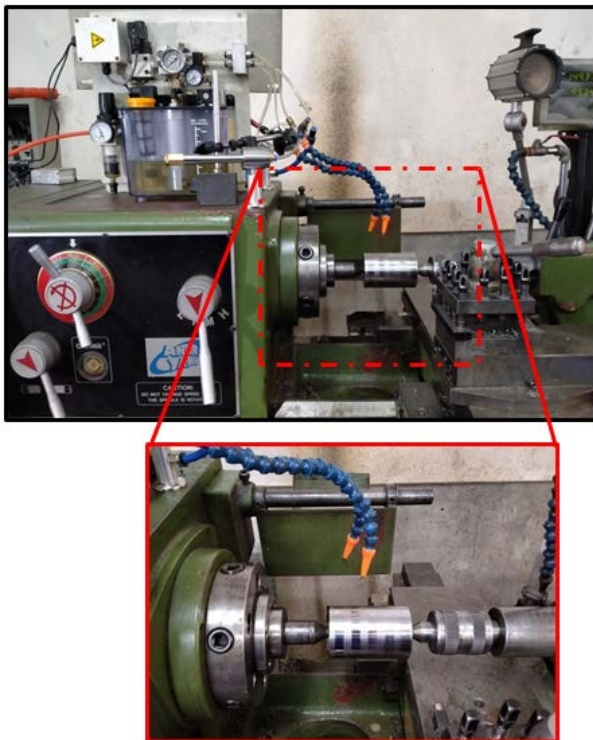
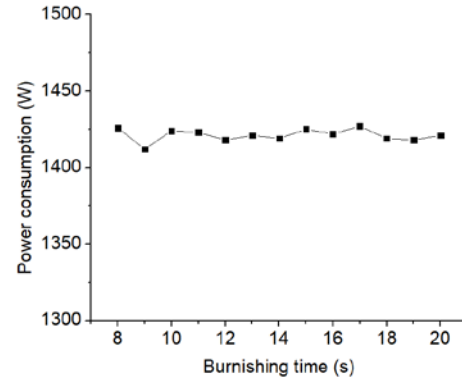
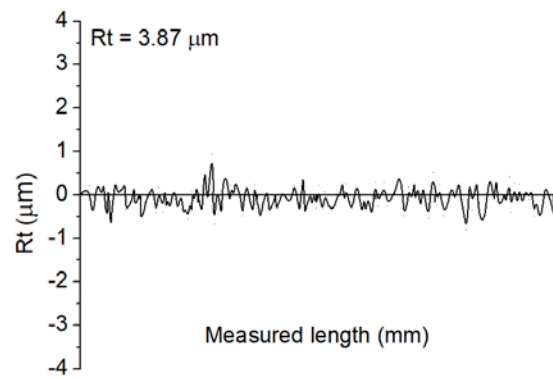


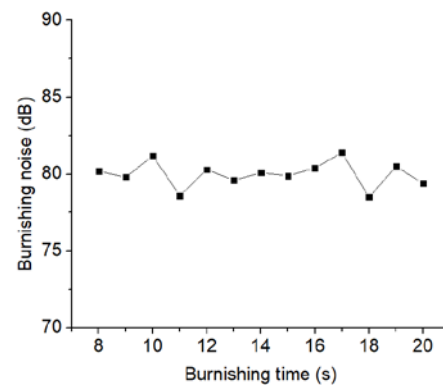
Fig. 3. The experimental setting



(a) The total power consumed



(b) The roughness profile



(c) The noise emission

Fig. 4. The representative values of burnishing responses

## 4 RESULTS AND DISCUSSIONS

### 4.1 Parametric influences

Table 3 presents experimental data for the burnishing operation.

As the  $D$  increases (1 mm to 3 mm), the  $ED$  is increased by 16.7% (Fig. 5a). A low  $D$  causes a low quantity of the mixture, leading to higher friction and greater resistance. More reactive energy is consumed; hence, the  $ED$  decreases. A higher  $D$  increases a higher amount of lubricant, leading to a reduction in the frictional coefficient. Consequently, lower total energy consumption is obtained, resulting in higher energy efficiency.

As the  $S$  increases (15 mm to 45 mm), the  $ED$  is decreased by 12.5% (Fig. 5b). A low  $N$  causes a low droplet diameter and higher fluid flow speed; hence, more oil mist penetrates the interfaces. The total energy consumption decreases; hence, the  $ED$  enhances. A higher  $N$  increases the droplet diameter and decreases the flow speed, leading to low heat dissipation impact. Higher friction is produced and low  $ED$  is generated.

Table 3. Experimental data

No.	D (mm)	S (mm)	P (deg.)	ED (%)	Rt ( $\mu$ m)	NE (dB)
Experimental data for developing ANN models						
1	1	15	30	24.02	4.42	83.8
2	1	30	30	23.33	5.09	88.1
3	1	45	30	20.97	5.78	95.5
4	1	15	45	25.86	4.01	79.4
5	1	30	45	25.21	4.66	82.9
6	1	45	45	22.91	5.32	89.5
7	1	15	60	25.32	4.57	83.9
8	1	30	60	24.71	5.18	86.6
9	1	45	60	22.45	5.83	92.5
10	2	15	30	25.66	3.87	80.3
11	2	30	30	24.99	4.49	84.2
12	2	45	30	22.66	5.14	91.2
13	2	15	45	27.32	3.47	75.6
14	2	30	45	26.69	4.06	78.7
15	2	45	45	24.42	4.68	84.9
16	2	15	60	26.63	4.03	79.8
17	2	30	60	26.01	4.62	82.1
18	2	45	60	23.76	5.19	87.6
19	3	15	30	27.79	3.16	77.2
20	3	30	30	27.14	3.73	80.7
21	3	45	30	24.82	4.34	87.3
22	3	15	45	29.26	2.77	72.1
23	3	30	45	28.65	3.31	74.8
24	3	45	45	26.38	3.89	80.7
25	3	15	60	28.35	3.33	76.1
26	3	30	60	27.78	3.85	77.9
27	3	45	60	25.56	4.41	83.2
Experimental data for testing ANN models						
28	2	25	35	25.56	4.42	83.2
29	1	25	55	26.22	4.03	79.8
30	3	35	40	25.54	4.69	83.6
31	1	20	50	27.83	3.54	77.5
32	2	40	40	25.92	4.31	80.6
33	3	20	50	25.03	4.52	83.5
34	1	35	35	29.21	3.02	72.9
35	2	22	55	23.62	5.06	87.4

Table 4. Computed ANOVA results for the  $ED$ 

So.	SS	MS	F Value	p-value
Model	51.335	5.704	35.601	< 0.0001
$D$	183.278	183.278	1143.929	< 0.0001
$S$	155.661	155.661	971.556	< 0.0001
$P$	54.177	54.177	338.148	< 0.0001
$DP$	19.689	19.689	122.888	0.0043
$D^2$	26.032	26.032	162.476	0.0031
$S^2$	88.468	88.468	552.171	< 0.0001
$P^2$	126.788	126.788	791.348	< 0.0001
Re.	1.122	0.160		
Cor.	52.457			
$R^2 = 0.97862$				
So.: Source; Re.: Residual; Cor.: Cor total				

Table 5. Computed ANOVA results for the  $R_t$ 

So.	SS	MS	F Value	p-value
Model	7.457	0.829	38.905	< 0.0001
$D$	16.050	16.050	753.510	< 0.0001
$S$	14.521	14.521	681.747	< 0.0001
$P$	1.282	1.282	60.174	0.0035
$DS$	1.135	1.135	53.265	0.0039
$SP$	0.655	0.655	30.756	0.0086
$D^2$	1.999	1.999	93.827	0.0027
$P^2$	11.488	11.488	539.336	< 0.0001
Re.	0.149	0.021		
Cor.	7.606			
$R^2 = 0.9804$				

Table 6. Computed ANOVA results for the  $NE$ 

So.	SS	MS	F Value	p-value
Model	406.501	45.167	33.790	< 0.0001
$D$	1336.101	1336.101	999.559	< 0.0001
$S$	1551.750	1551.750	1160.890	< 0.0001
$P$	348.624	348.624	260.811	< 0.0001
$DS$	126.615	126.615	94.722	0.0032
$DP$	107.536	107.536	80.449	0.0038
$SP$	257.276	257.276	192.472	0.0015
$S^2$	518.599	518.599	387.973	< 0.0001
$P^2$	1481.216	1481.216	1108.122	< 0.0001
Residual	9.357	1.337		
Cor Total	415.858			
$R^2 = 0.9775$				

As the  $P$  increases (30 deg. to 45 deg.), the  $ED$  is increased by 7.9%. As the  $P$  increases (45 deg. to 60 deg.), the  $ED$  is decreased by 3.9% (Fig. 5c). A lower  $P$  causes a low quantity of the lubricant due to an improper position of the nozzle, leading to high friction; hence, the  $ED$  decreases. A higher  $P$  causes more fluid participation; hence, the  $ED$  increases. Excessive  $P$  value causes a low quantity of lubricant; hence, the  $ED$  decreases.

As the  $D$  increases (1 mm to 3 mm), the  $R_t$  is decreased by 28.1% (Fig. 6a). A low  $D$  decreases the quantity of the mixture, resulting in high friction at the interfaces. More energy is consumed to burnish the workpiece; hence, a higher  $R_t$  is obtained. A higher  $D$  causes a higher quantity of the lubricant; leading to a reduction in the friction; hence, the  $R_t$  decreases.

As the  $S$  increases (15 mm to 45 mm), the  $R_t$  is decreased by 31.8% (Fig. 6b). A low  $S$  increases the heat dissipation effect due to the small size and high velocity of the mixture. The friction at the interfaces reduces and a low  $R_t$  is obtained. A higher distance causes a higher size and slow speed of the mixture, leading to low heat dissipation. Higher friction at the burnishing zone is generated and a higher  $R_t$  is produced.

As the  $P$  increases (30 deg. to 45 deg.), the  $R_t$  is decreased by 8.9%. As the  $P$  increases (45 deg. to 60 deg.), the  $R_t$  is increased by 14.9% (Fig. 6c). Further angle enhances cooling-lubrication impact when the proper position of the nozzle is set. More mixture is transferred into the burnishing region; hence, the  $R_t$  decreases. Excessive angle causes an improper location of the nozzle, leading to a reduction in the lubricant; hence, the  $R_t$  increases.

As the  $D$  increases (1 mm to 3 mm), the  $NE$  is decreased by 8.3% (Fig. 7a). A low  $D$  causes a low quantity of the oil mist, leading to higher friction between; hence, the  $NE$  increases. A higher  $D$  decreases the friction due to a higher quantity of the mixture. The material is easily burnished; hence, the  $NE$  reduces.

As the  $S$  increases (15 mm to 45 mm), the  $NE$  is increased by 13.1% (Fig. 7b). The friction at interfaces decreases due to its small size and the high velocity of the mixture when a low  $N$  is applied. The cooling-lubrication impact increases and the material is easily burnished; hence, the  $NE$  decreases. A higher  $S$  causes a low cooling-lubrication impact due to the low speed of the mixture, leading to higher friction; hence, the  $NE$  logically increases.

As the  $P$  increase (30 deg. to 45 deg.), the  $NE$  is decreased by 4.2%. As the  $P$  increases (45 deg. to 60 deg.), the  $NE$  is increased by 4.1% (Fig. 7c). The friction at the interfaces decreases with an increased pitch angle; hence, the  $NE$  reduces. Further  $P$  value causes higher friction and resistance; hence, the  $NE$  increases.

#### 4.2 ANOVA findings for performance measures

Table 4 presents ANOVA findings for the  $ED$  model. The contributions of the  $D$ ,  $S$ , and  $P$  are 27.74%, 23.56%, and 8.20%, respectively. The contribution of the  $DP$  is 2.98%. The contributions of the  $D^2$ ,  $S^2$ , and  $P^2$  are 3.94%, 13.39%, and 19.19%, respectively. The  $R^2$  of 0.97862 indicates that the  $ED$  model is significant.

Table 5 presents ANOVA findings for the  $R_t$  model. The contributions of the  $D$ ,  $S$ , and  $P$  are 33.81%, 30.59%, and 2.70%, respectively. The contributions of the  $DS$  and  $SP$  are 2.39% and 1.38%, respectively. The contributions of the  $D^2$  and  $P^2$  are 4.21% and 24.20%, respectively. The  $R^2$  of 0.9804 indicates that the  $R_t$  model is significant.

Table 6 presents ANOVA findings for the *NE* model. The contributions of the *D*, *S*, and *P* are 23.11%, 26.84%, and 6.03%, respectively. The contributions of the *DS*, *DP*, and *SP* are 2.19%, 1.86%, and 4.45%, respectively. The contributions of the *S*<sup>2</sup> and *P*<sup>2</sup> are 8.97% and 25.62%, respectively.

### 4.3 Development of the optimal TBRFFNN model

The working inputs of the TBRFFNN model, including the *TN*, *TP*, *TT*, *TH*, and *TL* are shown in Table 7. The computational trials of the TBRFFNN are performed based on the parameter combination entitled Taguchi L<sub>18</sub>. As shown in Fig. 8, the optimizing outcomes of the *TN*, *TP*, *TT*, *TH*, and *TL* are 19, MSEREG, logsig, 3, and Learn GDM, respectively.

Table 8 indicates the comparative values at different points. As a result, the computed deviations of the *ED*, *Rt*, and *NE* lie from -1.67% to 0.98%, -0.67% to 0.98%, and -1.56% to 0.75%, respectively. The allowable errors revealed that the proposed TBRFFNN models ensure prediction accuracy.

The regression graphs of the TBRFFNN are illustrated in Fig. 9, in which the R values of the training, testing, and all stages are 0.98345, 0.99755, and 0.98734, respectively. Consequently, the developed TBRFFNN models can accurately approximate the burnishing responses.

### 4.4 Optimality produced by the TBRFFNN-CRITIC-DA

The computed weights of the *ED*, *Rt*, and *NE* are 0.31, 0.40, and 0.29, respectively. Three optimizing solutions generated by the DA are presented in Table 9. Fig. 10 presents optimization results generated by the DA. Therefore, the optimal data of the *D*, *S*, and *P* are 3 mm, 15 mm, and 45 deg., respectively. The *ED* is improved by 12.7%, respectively, while the *Rt* and *NE* are decreased by 3 4.4% and 9.1%, respectively.

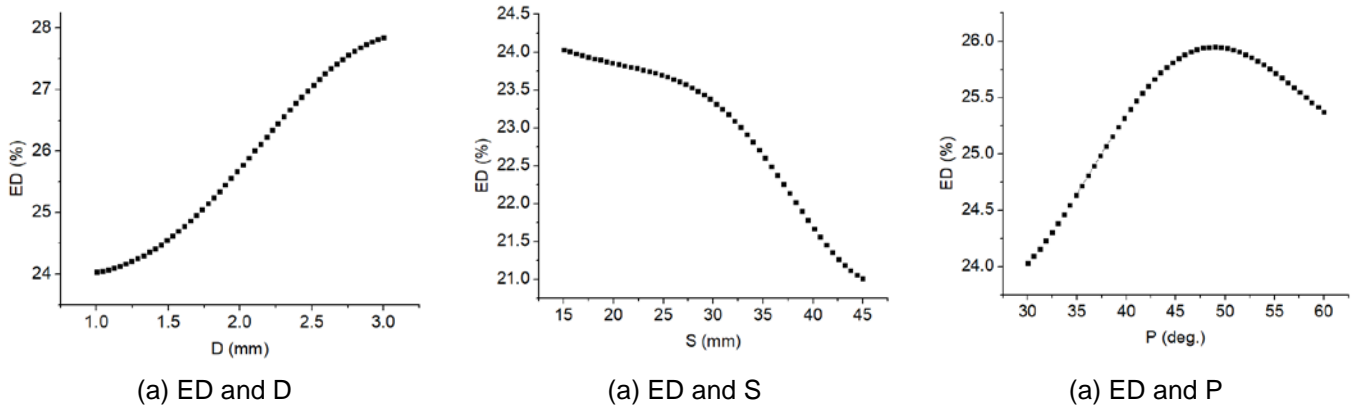


Fig. 5. The impacts of nozzle parameters on the ED

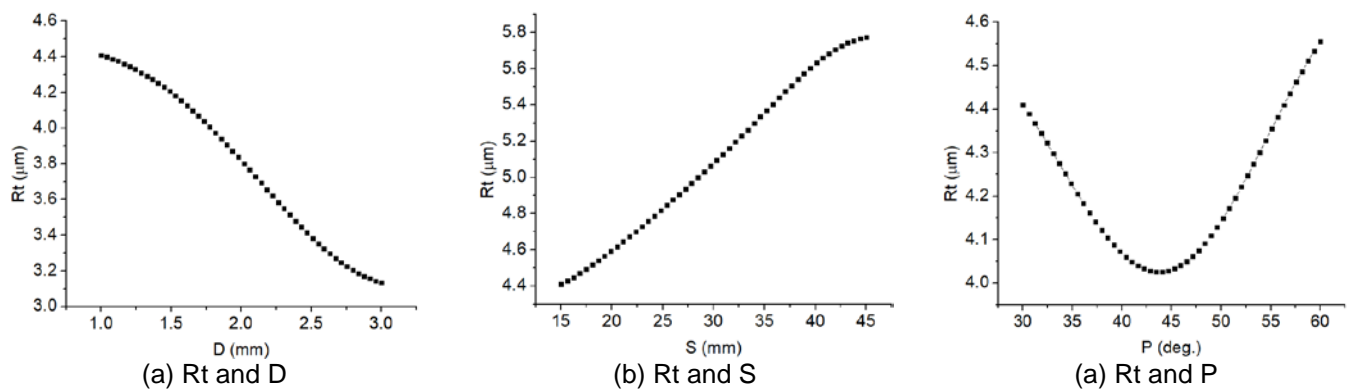


Figure 6. The impacts of nozzle parameters on the Rt

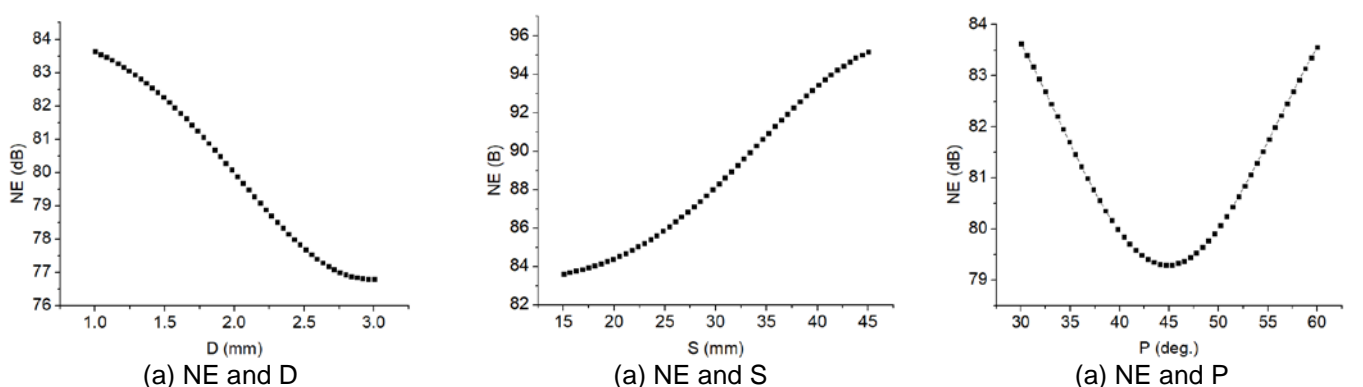


Fig. 7. The impacts of nozzle parameters on the NE

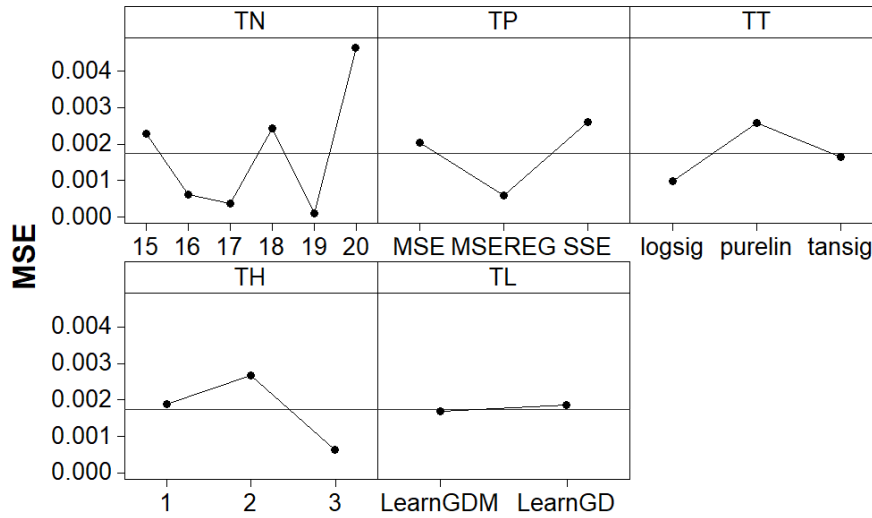


Fig. 8. The MSE values under different TBRFFNN parameters

Table 7. Operating parameters of the TBRFFNN models

Symbol	Parameters	Classifications
TN	The number of hidden neurons	15; 16; 17; 18; 19; 20
TP	Types of the performance function	MSE; MSEREG; SSE
TT	Types of the transfer function	Logsig; Purelin; Tansig
TH	The number of hidden layers	1; 2; 3
TL	Types of the learning function	Learn GDM; Learn GD

Table 8. Investigation of the precision of the developed TBRFFNN models

Responses		Experimental No.							
		28	29	30	31	32	33	34	35
Experiments	ED	25.56	26.22	25.54	27.83	25.92	25.03	29.21	23.62
	Rt	4.42	4.03	4.69	3.54	4.31	4.52	3.02	5.06
	NE	83.2	79.8	83.6	77.5	80.6	83.5	72.9	87.4
Predictions	ED	25.32	26.48	25.12	27.46	25.73	25.14	29.46	23.38
	Rt	4.43	4.05	4.72	3.56	4.29	4.49	3.05	5.08
	NE	84.5	79.2	83.1	77.9	80.2	83.1	73.4	87.9
Absolute errors (%)	ED	-0.95	0.98	-1.67	-1.35	-0.74	0.44	0.85	-1.03
	Rt	0.23	0.49	0.64	0.56	-0.47	-0.67	0.98	0.39
	NE	-1.56	0.75	0.60	-0.52	0.50	0.48	-0.69	-0.57

Table 9. Optimization results generated by the BRNN-CRITIC-DA

Method	Optimization parameters			Responses		
	D (mm)	S (mm)	P (deg)	ED (%)	Rt (µm)	NM (dB)
The values used	1.5	25	40	25.96	4.22	79.3
Optimal values	3.0	15	45	29.26	2.77	72.1
Improvement (%)				12.7	-34.4	-9.1

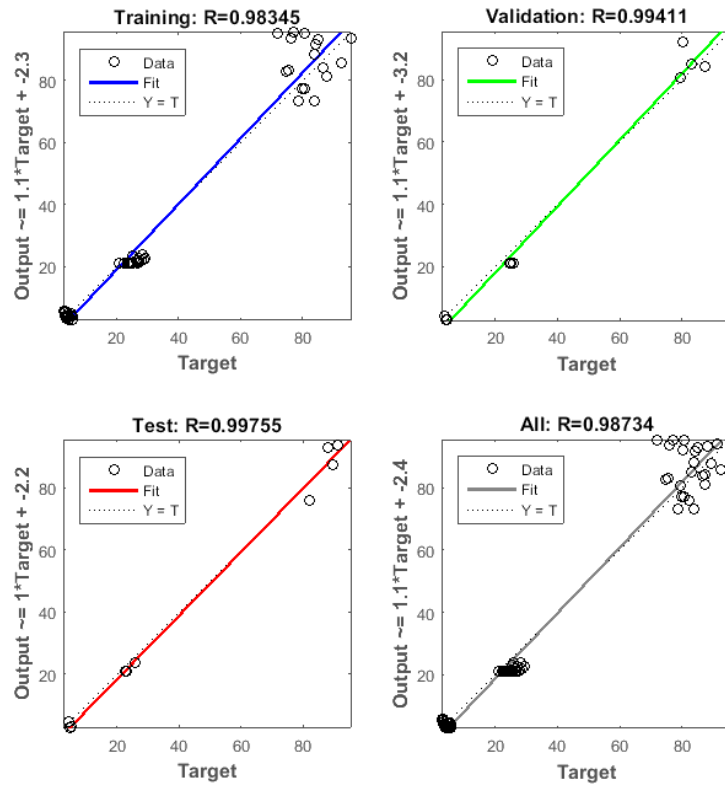


Fig. 9. Regression graphs for the TBRFFNN models

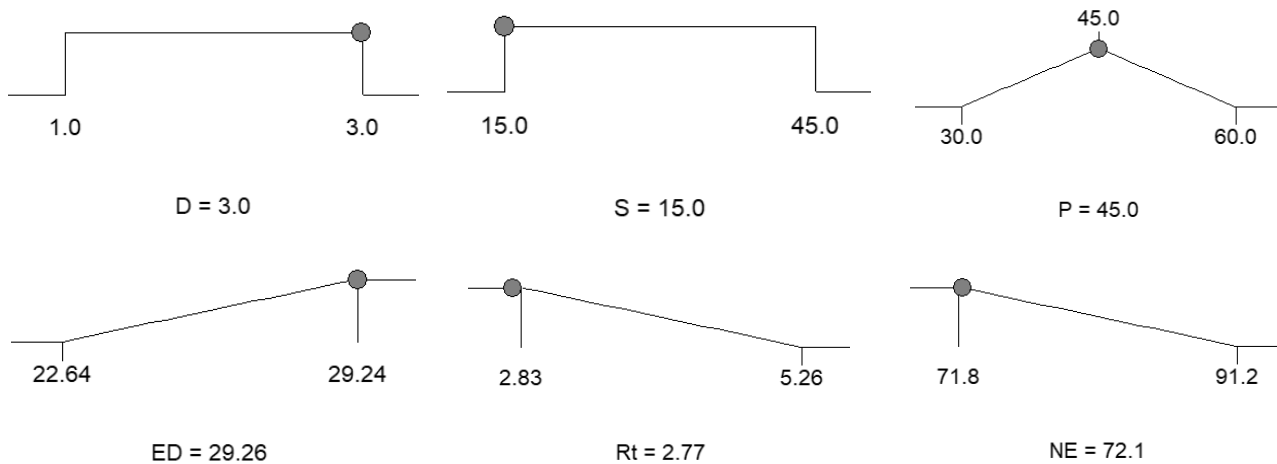


Fig. 10. Optimization results generated by the DA

#### 4.5 Academic and industrial contributions

The academic and industrial remarks are expressed as:

The optimization technique comprising the TBRFFNN, CRITIC, and DA could be utilized to deal with complex optimization issues for diamond burnishing and manufacturing processes.

The non-linear data of machining responses could be efficiently described using the TBRFFNN models.

The knowledge of the diamond burnishing process could be enhanced using the obtained results.

The proposed optimizing approach can be effectively applied to find optimal nozzle parameters for other machining processes.

The achieved outcomes could be used to boost the *ED* and decrease the *Rt* and *NE* for the diamond burnishing operation.

The MQL-assisted cooling-lubrication system can be effectively employed in other machining processes.

The TBRFFNN models of the *ED*, *Rt*, and *NE* could be utilized to calculate the machining responses in the practice.

## 5 CONCLUSIONS

In this study, the diamond burnishing operation was optimized to boost energy efficiency (*ED*), the total height of profile roughness (*Rt*) as well as noise emission (*NE*). The nozzle parameters are the inner diameter (*D*), the spraying distance (*S*), and the pitch angle (*P*). The response models were proposed using the TBRFFNN approach and optimal findings were determined with the support of the DA. The conclusions are expressed as:

1. To enhance the *ED*, the highest values of nozzle factors are recommended. To decrease the *Rt* and *NE*, a high diameter can be applied, while low distance and pitch angle are suggested.
2. For the *ED* model, the *D* had the highest impact, followed by the *S* and *P*, respectively. For the *Rt*, the *D* had the highest impact, followed by the *D* and *P*, respectively. For the *NE*, the *S* had the highest impact, followed by the *D* and *P*, respectively.
3. The optimal data of the *D*, *S*, and *P* were 3 mm, 15 mm, and 45 deg., respectively. The *ED* was improved by 12.7%, while the *Rt* and *NE* were decreased by 34.4% and 9.1%, respectively.
4. This investigation considered the *ED*, *Rt*, and *NE*. The productivity and other surface properties will be addressed in the next work.

## 6 REFERENCES

- [1] Sachin. B., Narendranath, S., Chakradhar, D. (2018). Experimental evaluation of diamond burnishing for sustainable manufacturing. *Materials Research Express*, vol. 5, no. 10, 106514. DOI:10.1088/2053-1591/aadb0a
- [2] Sachin. B., Narendranath, S., Chakradhar, D. (2020). Application of desirability approach to optimize the control factors in cryogenic diamond burnishing. *Arabian Journal for Science and Engineering*, vol. 45, 1305–1317. DOI: 10.1007/s13369-019-04326-3
- [3] Sachin. B., Narendranath, S., Chakradhar, D. (2019). Selection of Optimal Process Parameters in Sustainable Diamond Burnishing of 17-4 PH Stainless Steel. *Journal of the Brazilian Society of Mechanical Sciences and Engineering*, vol. 41, 219. <https://doi.org/10.1007/s40430-019-1726-7>
- [4] Maximov, J.T., Duncheva, G.V., Anchev, A, P, et al. (2020). Smoothing, deep, or mixed diamond burnishing of low-alloy steel components-optimization procedures. *International Journal of Advanced Manufacturing Technology*, vol. 106, 1917–1929. DOI: 10.1007/s00170-019-04747-2
- [5] Maximov, J.T., Duncheva, G.V., Anchev, A, P, et al. (2020). Improvement in fatigue strength of 41cr4 steel through slide diamond burnishing. *Journal of the Brazilian Society of Mechanical Sciences and Engineering*, vol. 42, 197. DOI: 10.1007/s00170-019-04747-2
- [6] Maximov, J.T., Duncheva, G.V., Anchev, A, P, et al. (2022). Improvement in wear resistance performance of CuAl8Fe3 single-phase aluminum bronze via slide diamond burnishing. *Journal of Materials Engineering and Performance*, vol. 31, 2466-2478. DOI: 10.1007/s40430-020-02276-8
- [7] Maximov, J.T., Duncheva, G.V., Anchev, A, P, et al. (2021). Multi-objective optimization of the internal diamond burnishing process. *Materials and Manufacturing Processes*, vol. 37, no. 4, 428-436. DOI: 10.1080/10426914.2021.1981937
- [8] Felhő, C., Varga, G. (2022). CAD and FEM modelling of theoretical roughness in diamond burnishing. *International Journal of Precision Engineering and Manufacturing*, vol. 23, 375–384. DOI: 10.1007/s12541-022-00622-5
- [9] Duncheva, G.V., Maximov, J.T., Anchev, A.P. et al. (2022). Improvement in surface integrity of CuAl8Fe3 bronze via diamond burnishing. *International Journal of Advanced Manufacturing Technology*, vol. 119, 5885–5902 (2022). DOI: 10.1007/s00170-022-08664-9
- [10] Duncheva, G.V., Maximov, J.T., Anchev, A.P. et al. (2022). Enhancement of the wear resistance of CuAl9Fe4 sliding bearing bushings via diamond burnishing. *Wear*, vol. 510–511, 204491. DOI: 10.1016/j.wear.2022.204491
- [11] Maximov, J., Duncheva, G., Anchev, A., et al. (2022). Effect of diamond burnishing on fatigue behaviour of AISI 304 chromium-nickel austenitic stainless steel. *Materials*, vol. 15, 4768. DOI: 10.3390/ma15144768
- [12] Nguyen T.T., Le M.T. (2021). Optimization of internal burnishing operation for energy efficiency, machined quality, and noise emission. *International Journal of Advanced Manufacturing Technology*, vol. 114, 2115–2139. DOI: 10.1007/s00170-021-06920-y
- [13] Nguyen T.T., Le M.T. (2021). Optimization of the internal roller burnishing process for energy reduction and surface properties. *Strojniški vestnik – Journal of Mechanical Engineering*, vol. 67, no. 4, 167-179. DOI: 10.5545/sv-jme.2021.7106
- [14] Nguyen T.T., Nguyen T.A., Trinh Q.H. et al. (2022). Multi-performance optimization of multi-roller burnishing process in sustainable lubrication condition. *Materials and Manufacturing Processes*, vol. 37, no. 4, 407-427. DOI: 10.1080/10426914.2021.1962533

- [15] Nguyen T.T., Le, V.A. (2022). Machining and optimization of the external diamond burnishing operation. Materials and Manufacturing Processes. DOI: 10.1080/10426914.2022.2072880
- [16] Đinh V.D., Vu D.Q. (2022). A mathematical model for thinning rate prediction of sheet double hydro-forming. Journal of Applied Engineering Science, Vol. 20, no. 3, 987-999. DOI: 10.5937/jaes0-35082
- [17] Buzauova, T., Turekhanov, B., Mateshov, A., et al. (2022). Planning and experimental studies of selection the optimal welding mode by the friction of fitting rods. Journal of Applied Engineering Science, Vol. 20, no. 3, 727-735. DOI: 10.5937/jaes0-35874
- [18] Srinivas, D., Sharma, S., Gowrishankar., et al. (2022). Optimization and prediction of the hardness behaviour of LM4 + Si3N4 composites using RSM and ANN - a comparative study. Journal of Applied Engineering Science, Vol. 20, no. 4, 1214-1225. DOI: 10.5937/jaes0-38109
- [19] Hidayat, H.F., Setiawan, R., Dhelika, R., et al. (2022). Investigation of relative influence of process variables in a 10-kW downdraft fixed-bed gasifier with ann models. Journal of Applied Engineering Science, Vol. 20, no.3, 971-977 (2022). DOI: 10.5937/jaes0-34344

*Paper submitted: 25.12.2022.*

*Paper accepted: 12.03.2023.*

*This is an open access article distributed under the CC BY 4.0 terms and conditions*